Defect ordering in epitaxial α-GaN(0001)

H. Z. Xiao, N.-E. Lee, R. C. Powell,[a] Z. Ma, L. J. Chou,[b] L. H. Allen, J. E. Greene, and A. Rockett

The Coordinated Science Laboratory, the Materials Research Laboratory, and the Department of Materials Science, University of Illinois, Urbana, Illinois 61801

(Received 26 May 1994; accepted for publication 6 September 1994)

The microstructure of nominally undoped epitaxial wurtzite-structure α-GaN films, grown by gas-source molecular-beam epitaxy, plasma-assisted molecular-beam epitaxy, and metalorganic chemical-vapor deposition, has been investigated by transmission electron microscopy (TEM) and high-resolution TEM. The results show that undoped α-GaN films have an ordered point-defect structure. A model of this defect-ordered microstructure, based upon a comparison between experimental results and computer simulations, is proposed. © *1994 American Institute of Physics.*

GaN has attracted considerable attention for use in blue to ultraviolet light emitting devices.[1–4] Recently, single-crystal GaN thin films have been successfully synthesized by a number of methods, including gas-source molecular-beam epitaxy (GSMBE),[5] reactive-ion MBE (RIMBE),[6] plasma-assisted MBE (PAMBE),[7–9] halide chemical-vapor deposition (CVD),[10] and metalorganic CVD (MOCVD).[11–13] However, it has been found to be difficult to control film electrical properties. Undoped wurtzite-structure α-GaN is usually n-type with a high concentration of shallow donors attributed to N vacancies,[10,14] a low electron mobility,[15] and a relatively low resistivity.[15] The properties of lattice defects in α-GaN are not understood.

In this communication, we report observations of the ordering of point defects in undoped α-GaN. The epitaxial films used in these experiments were grown on Al_2O_3 (0001)1×1 by GSMBE, PAMBE, and MOCVD. Transmission electron microscopy (TEM), high-resolution TEM, and electron diffraction show that ordering of defects in α-GaN occurs in clustered regions on alternating {0001} planes.

The experimental results presented here were obtained, unless otherwise noted, from nominally undoped epitaxial α-GaN films grown by GSMBE on Al_2O_3 (0001) substrates.[5] Similar results were obtained for all α-GaN samples examined including materials grown by GSMBE, PAMBE, and MOCVD. The experimental procedures for PAMBE and MOCVD have been described in detail in Refs. 9 and 11, respectively. For GSMBE, the substrates were degreased with successive rinses in trichloroethane, acetone, methanol, and isopropyl alcohol followed by a hot (160 °C) 3:1 H_2SO_4:H_3PO_4 acid etch. The substrates were then rinsed in de-ionized water, blown dry in dry N_2, inserted into the MBE system, and degassed at 800 °C. Ga and NH_3 fluxes were supplied from a standard temperature-controlled Ga effusion cell and a stainless-steel NH_3 doser,[5] respectively. The Ga flux was typically maintained at 7×10^{14} cm^{-2} s^{-1} (corresponding to a growth rate of ~0.5 μm/h) while the high-purity (99.9995%) NH_3 flux, regulated with a mass-flow controller, was $\sim1\times10^{17}$ cm^{-2} s^{-1}. Total film thicknesses ranged from 0.8 to 1.5 μm and growth temperatures T_s were 700–850 °C.

Post-deposition electron-diffraction and bright- and dark-field TEM imaging analyses were carried out in Philips EM420 and CM12 microscopes. High-resolution TEM experiments were performed using a Hitachi 9000 electron microscope operated at 300 kV. Plan-view and cross-sectional TEM samples were prepared by mechanically thinning to 50–80 μm followed by cold state (~77 K) ion milling to perforation using 5.5 kV Ar^+. The plan-view samples were thinned from the substrate side to minimize residual ion-induced damage in the films. Samples were also examined using a Rigaku double-crystal x-ray-diffraction (XRD) system.

The primary extended defects observed in as-grown α-GaN films, as shown in the typical bright-field cross-sectional TEM micrograph in Fig. 1(a), are threading dislocations (indicated by "d") and (0001) stacking faults (labeled by arrows). Note that the stacking fault contrast is low under the (0000)–(0002) two-beam imaging conditions used to obtain Fig. 1(a) since the fault planes are parallel to the electron beam. Contrast near the film/substrate interface arises primarily from misfit strain. The $[\bar{1}2\bar{1}0]_{GaN}$/$[01\bar{1}0]_{Al_2O_3}$ zone-axis diffraction pattern in Fig. 1(b), from both the film and substrate, shows the epitaxial relationship: GaN (0001)$\|Al_2O_3$ (0001) and GaN$[\bar{1}2\bar{1}0]\|Al_3O_3$ $[01\bar{1}0]$. This indicates that the GaN basal plane is rotated 30° with respect to that of the substrate, in agreement with previous results,[5] leading to a reduction in the mismatch from 33% to 16%. The residual misfit strains calculated from the diffraction pattern in Fig. 1(b) are −2.0% in the interface plane and +0.2% along the growth direction, indicating that most of the misfit strain has been relieved.

GaN [0001] plan-view and $[01\bar{1}0]$ and $[\bar{1}2\bar{1}0]$ cross-sectional zone-axis diffraction patterns are presented in Figs. 2(a)–2(c), respectively. These zone axes constitute the stereographic triangle [0001]–$[01\bar{1}0]$–$[\bar{1}2\bar{1}0]$ of the α-GaN wurtzite structure. In addition to wurtzite diffraction spots, streaking along the [0001] direction [see Figs. 1(b) and 2(c)] and {0001} forbidden reflections, marked by arrow heads in Figs. 2(b) and 2(c), were observed. The [0001] streaks are attributed to basal plane stacking faults.[16] Faults at various

[a]Current address: Solar Cells Inc., 1702 N. Westwood Ave., Toledo, OH 43607.

[b]The Department of Electrical and Computer Engineering and the Center for Compound Semiconductor Microelectronics, University of Illinois, 208 North Wright St., Urbana, IL 61801.

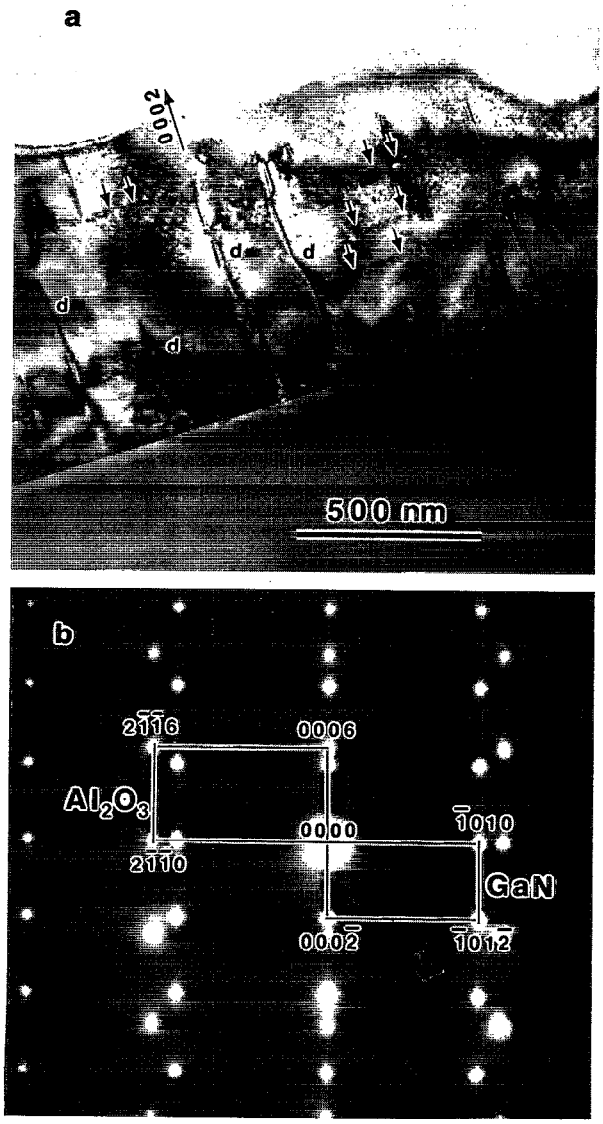

FIG. 1. (a) A bright-field TEM micrograph of GSMBE α-GaN. Threading dislocations are indicated by "d" and (0001) stacking faults are labeled by arrows. (b) A corresponding $[\bar{1}2\bar{1}0]_{GaN}+[01\bar{1}0]_{Al_2O_3}$ zone-axis diffraction patterns from both the film and the substrate. The basic units of the diffraction pattern due to Al_2O_3 (the larger rectangle) and GaN (the smaller rectangle) are indicated and the corner reflections of each are indexed.

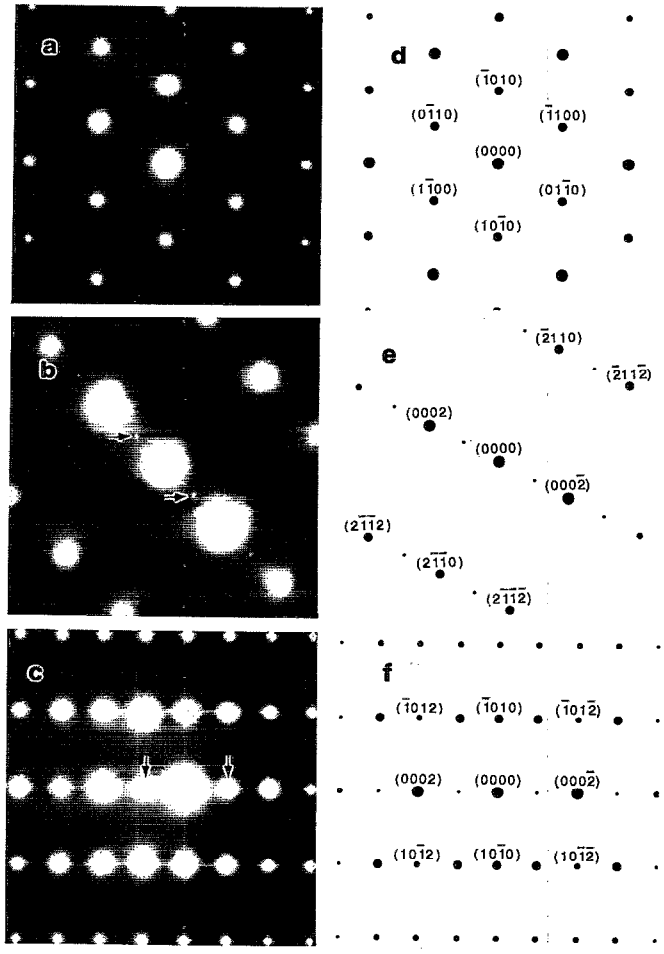

FIG. 2. Experimental and simulated zone-axis electron-diffraction patterns from GSMBE α-GaN. The zone axes are (a) and (d) [0001], (b) and (e) [01$\bar{1}$0], and (c) and (f) [$\bar{1}$2$\bar{1}$0], respectively.

separations give rise to a range of polytype orders ($2h$, $6h$,...,nh) which result collectively in a continuum of reflections along [0001]. The streaks in Fig. 1(b) are associated only with α-GaN reflections, and not with substrate reflections. Due to a shorter exposure time (in order to obtain increased contrast in the fundamental reflections), the streaks in Fig. 1(b) are much fainter than in Fig. 2(c), and the {0001} reflections are invisible.

High-resolution TEM images such as that in Fig. 3 show regions of alternating high and low intensity (0001) lattice fringes. The doubling of the [0001] lattice periodicity is localized in domains representing ~1% of the total volume and distributed randomly throughout the film. Intensity at (0001) was also observed in XRD scans obtained from single-crystal samples oriented to maximize the (0002) intensity. The (0001)/(0002) XRD peak intensity ratio was $\sim 10^{-6}$. We have observed the same diffraction and lattice image phenomena in α-GaN films grown by PAMBE and MOCVD.

In a perfect wurtzite lattice there is no allowed intensity at (0001) since diffracted waves from {0001} planes interfere destructively. This is the case whenever the structure factor is equal for all {0001} planes. Hence any change in the crystal structure that occurs equally on all {0001} planes will not give rise to diffracted intensity at (0001). Conversely, the observation of intensity at (0001) implies an ordered defect structure in which, for example, a net defect density occurs in the first, third, fifth,... {0002} planes and not in the second, fourth, sixth,... {0002} planes. Such a situation is shown schematically in Fig. 4.

The effect of changing the structure factor associated with the {0001} planes was simulated using the diffraction-simulation computer program DIFFRACT.[17] [0001], [01$\bar{1}$0], and [$\bar{1}$2$\bar{1}$0] zone-axis diffraction patterns were calculated [see Figs. 2(d)–2(f), respectively] assuming a random distri-

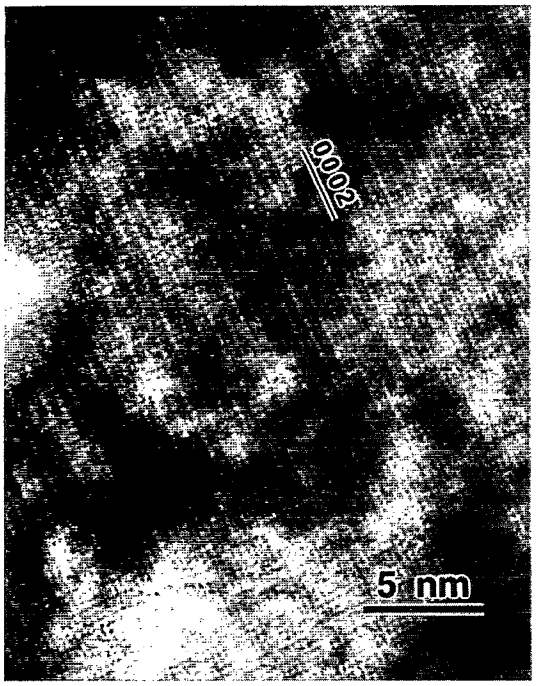

FIG. 3. A high-resolution TEM lattice image showing a domain consisting of alternate high intensity and low intensity (0001) basal plane fringes.

bution of defects (nitrogen vacancies in the simulation carried out here), on 0.5% of the lattice sites on alternate {0002} planes. Effects due to stacking faults were ignored. The stronger relative intensities of the observed (0001) forbidden reflections, labeled by an arrowhead in Fig. 2(c), compared to the computer simulation in Fig. 2(f), are due to double diffraction. This occurs at {0001} reflections in the $[\bar{1}2\bar{1}0]$ zone axis because the $\{101m\}$ and $\{000m\}$ reflections, where m is an integer, are related by a reciprocal lattice vector. No such effect is possible in the $[01\bar{1}0]$ zone axis. Thus the (0001) reflections in the $[01\bar{1}0]$ zone-axis diffraction pattern are entirely due to defect ordering. The 0.5% defect concentration used in the simulations was selected based on the relative intensities of the diffraction peaks in the XRD patterns.

Finally, we consider the relationship between the ordered defects and the carrier concentration observed in the materials. All of the samples examined were n-type with carrier concentrations of $1-4\times10^{18}$ cm^{-3}. This is much less than the concentration of defects estimated to be present in the samples. The electrical inactivity of the excess defects can be explained by their observed tendency to cluster. A reasonable assumption, based upon the low N activity during the film growth,[5,6] is that the defect clusters are predominantly nitrogen vacancies. However, other defects such as Ga on N antisite defects may also assist in providing charge compensation. The free-carrier concentration then results from point defects, presumably mostly vacancies, not captured in clusters and/or from partial activity of clustered defects. Vacancy ordering may also explain why the residual misfit along [0001] is smaller than would be expected from the combination of the Poisson effect and the residual strain in the plane of the interface.

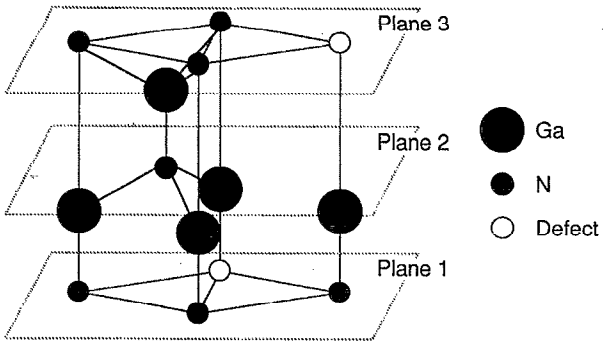

FIG. 4. A primitive wurtzite-structure α-GaN unit cell in which one N atom is replaced by a vacancy.

The authors acknowledge the financial support of the Electric Power Research Institute, the U. S. Department of Energy under Contract No. DEFG02-91-ER45439, the Joint Services Electronics Program, and SRC, and L. A. acknowledges a grant from the Petroleum Research Fund ACS-PRF No. 25422-G5 (Ref. No. 91-PRI-A-1729).

[1] T. Kawabata, T. Matsuda, and S. Koike, J. Appl. Phys. **56**, 2367 (1984).
[2] M. A. Khan, Microwave J. **36**, 67 (1993).
[3] H. Amano, T. Tanaka, Y. Kunii, K. Kato, S. T. Kim, and I. Akasaki, Appl. Phys. Lett. **64**, 1377 (1994).
[4] H. G. Lee, M. Gershenzon, and B. L. Goldenberg, J. Electron. Mater. **20**, 621 (1991).
[5] R. C. Powell, N.-E. Lee, and J. E. Greene, Appl. Phys. Lett. **60**, 2505 (1992).
[6] R. C. Powell, N.-E. Lee, Y.-W. Kim, and J. E. Greene, J. Appl. Phys. **73**, 189 (1993).
[7] C. R. Eddy, Jr. and T. D. Moustakas, J. Appl. Phys. **73**, 448 (1993).
[8] T. Lei, T. D. Moustakas, R. J. Graham, Y. He, and S. J. Berkowitz, J. Appl. Phys. **71**, 4933 (1992).
[9] M. E. Lin, B. Sverdlov, G. L. Zhou, and H. Morkoç, Appl. Phys. Lett. **62**, 3479 (1993).
[10] H. P. Marusha and J. J. Tietjen, Appl. Phys. Lett. **15**, 327 (1969).
[11] M. A. Khan, R. A. Skogman, R. G. Schulze, and M. Gershenzon, Appl. Phys. Lett. **43**, 492 (1983).
[12] T. Sasaki and S. Zembutsu, J. Appl. Phys. **61**, 2533 (1987).
[13] B.-C. Chung and M. Gershenzon, J. Appl. Phys. **72**, 651 (1992).
[14] D. W. Jenkins, J. D. Dow, and M. H. Tsai, J. Appl. Phys. **72**, 4130 (1992).
[15] R. J. Molnar, T. Lei, and T. D. Moustakas, Appl. Phys. Lett. **62**, 72 (1993).
[16] J. van Landuyt, R. Gevers, and S. Amelinckx, Phys. Status Solidi **18**, 167 (1966).
[17] The diffraction calculation program DIFFRACT is distributed by Virtual Laboratories, Albuquerque, NM.